Synergism between microRNA-124 and ELAVL3 drives neuronal gene upregulation during direct neuronal reprogramming of human fibroblasts

Ya-Lin Lu[1,2,3], Yangjian Liu[1,2], and Andrew S. Yoo[1,2*]

[1]Department of Developmental Biology, Washington University School of Medicine, St. Louis, MO 63110, USA

[2]Center for Regenerative Medicine, Washington University School of Medicine, St. Louis, MO 63110, USA

[3]Program in Developmental, Regenerative and Stem Cell Biology, Washington University School of Medicine, St. Louis, MO 63110, USA

[*]Correspondence: yooa@wustl.edu

Summary

Human neurons generated by direct conversion of adult fibroblasts can serve instrumental tools for modeling diseases as well as a platform to study neurogenic processes. Neuron-enriched microRNAs (miRNAs), miR-9/9* and miR-124 (miR-9/9*-124), direct cell fate switching of human fibroblasts to neurons when ectopically expressed. A critical component of the miRNA-mediated conversion process is the role of miR-9/9*-124 targeting and repressing anti-neurogenic genes. However, how these miRNAs function beyond the onset of the neuronal program remains unclear. Here, we performed the Argonaute (AGO) HITS-CLIP analysis to map direct target transcripts of miR-9/9*-124 when cells start adopting the neuronal fate during the conversion (reprogramming) process. Surprisingly, we found that miR-124, in particular, targets a suite of genes associated with neuronal differentiation and function, and these targets appeared

to be upregulated by miR-124, as knocking down miR-124 function diminished the expression of these targets. A critical example of the upregulated miR-124 target genes is *PTBP2*, a neuron-enriched RNA-binding protein known to be repressed by its homolog PTBP1. We elected to focus on *PTBP2* to gain insights into the mechanism underlying the activity of miR-124 as an inducer of its target genes. Paradoxically, both *PTBP1* and *PTBP2* are repressive targets of miR-124 in non-neuronal cells, yet PTBP2 selectively escapes the repression and becomes enriched in neurons. By interrogating 3'UTR sequences of *PTBP1* and *PTBP2*, we provide evidence that the switching of miR-124 activity to an activator is determined by the sequence availability at the target transcript that allows the binding of neuronal RNA-binding proteins, in particular ELAVL3 for select upregulation of PTBP2. ELAVL3 binds and interacts with AGO at PTBP2 3'UTR, yet ELAVL3 binding alone without miR-124 sites is insufficient to trigger the upregulation of PTBP2. Knocking down ELAVL3 expression during neuronal reprogramming leads to PTBP2 downregulation and impairs neuronal conversion, highlighting the concerted interplay between miR-124 and ELAVL3 that drives neuronal fate acquisition. By elucidating how miR-124 promotes PTBP2 induction, our study lends support to the underexplored role of miRNAs in promoting target gene expression in neurons.

Introduction

MiR-9/9* and miR-124 (miR-9/9*-124) are efficient reprogramming effectors that, when ectopically expressed in human adult fibroblasts (HAFs), induce an extensive reconfiguration of the chromatin accessibility landscape leading to the erasure of fibroblast fate and activation of the neuronal program (Abernathy et al. 2017). The conversion process by miR-9/9*-124 shares similarities to molecular cascades underlying neurogenesis during neural development such as the downregulation of REST, a well-established transcription repressor of neuronal genes (Ballas

48 et al., 2005; Lee et al., 2018; Schoenherr and Anderson, 1995) and switching of homologous
49 chromatin modifiers from non-neuronal to neuronal counterparts including DNMT3B to
50 DNMT3A, subunits of BAF/BRM-associated factor (BAF) complexes, and TOP2A to TOP2B
51 (Abernathy et al. 2017; Lee et al. 2018; Lessard et al. 2007; Staahl et al. 2013; Watanabe et al.
52 1994; Yoo et al. 2009; Tsutsui et al. 2001). Although the direct repression by brain-enriched
53 miRNAs on non-neuronal targets, for instance, *REST* (Packer et al., 2008; Visvanathan et al.,
54 2007), *ACTL6A* (Yoo et al., 2009), and *PTBP1* (Makeyev et al., 2007) for the induction of
55 neuronal counterparts offer a classic representation of miRNAs acting as negative regulators of
56 downstream target genes, how these miRNAs function in the midst of neuronal milieu remains
57 unknown.

58 The robustness of miRNA-based neuronal reprogramming allows for the investigation of
59 the pathways downstream of miR-9/9*-124 that promote neuronal identity (Abernathy et al.
60 2017). In the present study, we employed high-throughput sequencing of RNA isolated by
61 crosslinking immunoprecipitation (HITS-CLIP) of Argonaute (AGO) during miR-9/9*-124-
62 mediated neuronal reprogramming of human fibroblasts to map miR-9/9*-124-target interactions
63 at the onset of neuronal fate acquisition. Unexpectedly, we identified a suite of neuronal genes
64 enriched with AGO binding, in particular, corresponding to the binding sites of miR-124. The
65 upregulation of these neuronal genes required miR-124, suggesting that miR-124 not only
66 function as a repressor, but also as an effector to promote neuronal gene expression. Although
67 the ability of miRNAs as a positive effector of downstream target genes has been implicated
68 before (Truesdell et al., 2012; Vasudevan et al., 2007; Vasudevan and Steitz, 2007), little is
69 known about the molecular mechanism that governs a miRNA's activity as an activator in
70 neurons.

71 Among the genes identified to be targeted and upregulated by miR-124 was *PTBP2*, a
72 neuron-enriched RNA-binding protein (RBP). We elected to further focus on *PTBP2* to
73 understand the mechanism underlying miR-124 as an activator because the miR-124-PTBP2 axis
74 presented intriguing questions. A non-neuronal homolog *PTBP1* (Boutz et al., 2007) and *PTBP2*
75 both contain miR-124 target sites at their 3'UTRs (Makeyev et al., 2007; Xue et al., 2016). Why
76 is there selective repression on *PTBP1* while *PTBP2* escapes the repression by miR-124 in
77 neurons? The current view on the initial activation of *PTBP2* points to the activity of PTBP1 as a
78 repressor of *PTBP2* that is relieved upon miR-124 expression at the onset of neuronal
79 differentiation (Makeyev et al., 2007). However, the mechanism by which *PTBP2* expression
80 persists while being targeted by miR-124 remains unknown. In this study, we describe a series of
81 experiments to provide evidence for an RNA-binding protein, ELAVL3, induced during
82 neuronal conversion, directly acting on *PTBP2* 3'UTR to mediate the mode of miR-124 as an
83 activator, and the synergism between miR-124 and ELAVL3 that drives the neuronal conversion
84 of human fibroblasts.
85
86 **Results**
87 **AGO binds both downregulated and upregulated genes during miR-9/9*-124-mediated**
88 **direct neuronal reprogramming of human fibroblasts**
89 We have previously shown that ectopically expressing miR-9/9*-124 in human adult fibroblasts
90 (HAFs) induced a neuronal state characterized by the appearance of neuronal markers (such as
91 MAP2, TUBB3, NCAM, and SNAP25) (Figure 1A) and electrical excitability (Abernathy et al.
92 2017). To infer the role of miR-9/9*-124 as converting cells acquire the neuronal identity, we
93 carried out AGO HITS-CLIP after two weeks into reprogramming, a time point when neuronal
94 genes start being activated (Abernathy et al. 2017), to identify transcripts bound with AGO

95 loaded with miR-9/9* or miR-124 over the non-specific miRNA (miR-NS) control ($Log_2FC \geq 2$;
96 adj.P-value < 0.05). We then compared these hits to the list of differentially expressed genes
97 (DEGs) (by RNA-seq analysis; $-2 \leq Log_2FC \geq 2$; adj.P-value < 0.05) at day 20 of miRNA-
98 induced neurons (miNs) (Abernathy et al. 2017). As expected, we found target transcripts that
99 were downregulated consistent with the repressive mode of miRNAs (Figure 1B, 123 genes
100 labeled as green dots). Some of these are known targets of miR-124, such as *SOX9* (Farrell et al.
101 2011), *TEAD1* (Mucaj et al., 2015; Sun et al., 2015), and *VAMP3* (Chen et al. 2019).
102 Interestingly, we also discovered 301 unique gene transcripts with enriched AGO binding, which
103 were upregulated in day 20 miNs (Figure 1B, red dots). By gene ontology (GO) analysis, these
104 upregulated genes were associated with various neuronal processes such as synaptic transmission
105 and neuronal differentiation (red) in contrast to downregulated target genes (green) (Figure 1C).
106 Moreover, when examined against the time-course transcriptome analysis during neuronal
107 reprogramming (Abernathy et al. 2017), the expression of the identified neuronal target genes
108 showed continuous upregulation during the later time point of neuronal conversion (Figure 1D).
109 For example, transcripts of neuronal genes such as *MAP2*, *PTBP2*, and *SLC4A8* that were highly
110 expressed in day 20 miNs harbored AGO binding containing (Figure 1E). To determine the
111 fraction of upregulated neuronal genes that are likely actual targets of miR-9/9* and/or miR-124,
112 we extracted the AGO-enriched sequences and predicted the duplex formation by either miR-
113 9/9* and/or miR-124 through RNAhybrid (a maximum free energy threshold of -20 kcal/mol)
114 (Rehmsmeier, 2004). Of the 301 upregulated DEGs in miNs bound by AGO (Figure 1B), 261
115 (~86%) gene transcripts are predicted to contain miR-9/9* and/or miR-124 binding sites (Figure
116 1F). These transcripts harboring miR-9/9*-124 sites are also associated with various neuronal
117 GO terms such as in neuronal differentiation and synaptic processes (Figure 1F) as they include a
118 selection of neuronal genes identified earlier (Figures D-E). Of these upregulated miR-9/9*-124

119 target genes (in which approximately a half harboring target sites for both miR-9/9* and miR-
120 124), more than 90% of the total genes (240 genes) contain miR-124 target sequence, while less
121 than 60% of the genes (147 genes) contain miR-9/9* target sites (Figure 1G). These results
122 collectively demonstrate that the AGO-loaded transcripts differentially (up or down) respond to
123 miR-9/9*-124 during the neuronal conversion.
124
125 **MiR-124 target genes are upregulated during neuronal conversion**
126 As a larger fraction of the upregulated genes are predicted to contain miR-124 target sequences
127 (Figure 1G), we further tested if the upregulated genes were *bona fida* miR-124 targets by
128 knocking down miR-124 expression through the use of a tough decoy to inhibit the miRNA
129 activity (Bak et al., 2013; Haraguchi et al., 2009). The effect of the lentivirus-based tough decoy
130 for miR-124 (TuD-miR-124) was monitored after transduction by following the concurrent RFP
131 reporter expression and measuring the mature miR-124 level. TuD-miR-124 yielded more than
132 60% reduction of miR-124 expression in comparison to the control, non-specific miRNA tough
133 decoy (TuD-miR-NS) (Figure S1A-S1B). We then performed RNA-seq analysis on day 20 miNs
134 treated with either TuD-miR-NS or TuD-miR-124 to identify genes that fail to be upregulated
135 with TuD-miR-124 (Figure 2A, S1C) ($Log_2FC \leq 0.5$; adj.P-value < 0.01). When compared with
136 upregulated DEGs in day 20 miNs that were also enriched for AGO binding (Figure 1), we
137 identified 118 genes that failed to be upregulated upon miR-124 reduction (Figure 2A, Table S1).
138 With GO analysis, these identified genes were associated with neuronal terms such as neuronal
139 development and synaptic activity (Figure 2B).
140 To further analyze the miR-124 and target interactions, we looked into the potential
141 duplex formations between miR-124 and the identified AGO HITS-CLIP peak regions using
142 RNAhybrid (a maximum free energy threshold of -20 kcal/mol) (Rehmsmeier, 2004). From the

143 3’UTR sequences of the 118 genes, we identified a spectrum of miR-124 and target 3’UTR
144 duplex configurations from the canonical 2-8 seed base pairing to non-canonical base pairing
145 starting at position 3 and 4 (Figures 2C, S1D, and S2). These examples include *MAP2* 3'UTR, in
146 which miR-124 base pairing is predicted to start at position 3, while miR-124 target sequences
147 on *PTBP2* 3’UTR at the two peaks are predicted to start at position 1 and position 2, respectively
148 (Figure 2C). Interestingly, across the predicted miR-124:target duplex configurations, we
149 observed consistent auxiliary 2-3 base pairing at the 3’ end of miR-124 (Figure S1D).
150 Our results so far support the notion that miR-124 can target and promote the expression
151 of select neuronal genes when cells acquire the neuronal fate during neuronal conversion. We
152 wondered if the active mode of miR-124 on neuronal genes can be recapitulated in non-neuronal
153 cell types. We cloned the 3’UTRs of the identified neuronal target genes into a luciferase
154 reporter construct and transfected into a non-neuronal cell type, HEK293T (a human embryonic
155 kidney cell line), with a miR-9/9*-124 expression construct. After 48 hours post-transfection, we
156 found that unlike miRNA-induced neurons, miR-9/9*-124, instead, led to the repression of the
157 luciferase signal in HEK293T cells in comparison to the control miR-NS, while the non-target
158 control, *PGK1* 3’UTR was unaffected (Figure 2D). This result suggests that additional
159 determinants available in neuronal cells may be in play to govern the activity of miR-124 as a
160 positive regulator while simultaneously functioning to repress non-neuronal targets (Figure 2E).
161

162 **PTBP1 and PTBP2 3’UTR as targets of miR-124**

163 To further dissect the mechanism underlying the dual modes of miR-124 on its targets, we
164 elected to focus on *PTBP2* from the list of our identified neuronal targets because i) *PTBP2* and
165 its non-neuronal homolog, *PTBP1*, both contain miR-124 sites in their 3’UTRs (Figure 3A), and
166 ii) both *PTBP1* and *PTBP2* 3’UTRs are targeted and repressed by miR-124 in HEK293T cells

167 (Figure 3A), and iii) contrastingly, as observed in the human brain, the neuronal conversion
168 establishes the mutually exclusive expression between *PTBP1* and *PTBP2* (Figure 3B).
169 Therefore, the PTB homologs represent an ideal example to investigate how two closely related
170 targets respond differently to miR-124.

171 The 3'UTRs of human *PTBP1* and *PTBP2* contain two predicted target sites for miR-124
172 (yellow bar) and one site for miR-9 (blue bar) (Figure 3A). Luciferase reporter assays in the non-
173 neuronal HEK293T cells showed that miR-9/9*-124 or miR-124 alone (but not miR-9/9* alone)
174 was sufficient to repress both *PTBP1* and *PTBP2* through their 3'UTRs indicating that miR-124
175 is the primary miRNA targeting both PTB 3'UTRs (Figure 3A). Moreover, mutating the two
176 miR-124 sites in *PTBP2* 3'UTR (s1 and s2) rendered the 3'UTR insensitive to miR-124 (Figure
177 S3A). While our results pointing to the ability of miR-124 to target and repress 3'UTRs of both
178 *PTBP1* and *PTBP2* in cell lines were consistent with previous findings (Makeyev et al., 2007;
179 Xue et al., 2016), miRNA-mediated neuronal conversion of HAFs establishes the mutually
180 exclusive expression of PTBP1 and PTBP2 (Figure 3B), as *in vivo* neurons (Boutz et al., 2007).

181 Because *PTBP1* and *PTBP2* are regulated oppositely in miNs, we asked whether the
182 repressive activity of miR-124 on *PTBP2* 3'UTR could be reversed with a prolonged neurogenic
183 input by miR-9/9*-124 in HEK293T cells. We expressed a destabilized EGFP reporter
184 containing *PTBP1* 3'UTR, *PTBP2* 3'UTR, or control 3'UTR (CTL) that lacks a 3'UTR in
185 HEK293T cells with the miR-9/9*-124 expression construct (Figure SB). Analogous to PTBP2
186 upregulation during neuronal reprogramming of HAFs, we observed the selective increase in
187 EGFP expression with *PTBP2* 3'UTR within ten days of miR-9/9*-124 expression, contrasting
188 the continued repression of EGFP with *PTBP1* 3'UTR (Figures S3B-C). These results suggest
189 that with the prolonged neurogenic input, *PTBP2* 3'UTR responds to miR-124 differentially
190 from when measured after 48 hours with miRNA expression in HEK293T cells (Figure 3A).

191

192 **MiR-124 accentuates PTBP2 expression beyond the induction mediated by the**

193 **downregulation of PTBP1**

194 Previous studies have shown that during development, PTBP1 destabilizes *PTBP2* transcript in

195 non-neuronal cells by alternative splicing, and at the onset of neurogenesis, miR-124 directly

196 represses *PTBP1* resulting in PTBP2 induction (Boutz et al., 2007; Makeyev et al., 2007). Upon

197 miR-9/9*-124 expression in HAFs, we observed the concomitant downregulation and

198 upregulation of endogenous PTBP1 and PTBP2, respectively. As expected, the initial PTBP2

199 upregulation was abrogated when *PTBP1* cDNA was overexpressed (Figure 3C), supporting the

200 role of PTBP1 reduction as the initiation step of PTBP2 expression. We then sought to stratify

201 the contribution of PTBP1 repression alone versus the input of miRNAs to the overall PTBP2

202 level. When PTBP2 protein levels were compared between PTBP1 knockdown with a short

203 hairpin RNA (shRNA) and miR-9/9*-124 expression, we found that miR-9/9*-124 enhanced the

204 PTBP2 level by nearly a two-fold increase over the PTBP1 knockdown alone condition (Figure

205 3D). In fact, PTBP2 was more upregulated with miR-9/9*-124 despite the more pronounced

206 reduction of PTBP1 with shRNA (Figure 3D), demonstrating that miR-9/9*-124 accentuate

207 PTBP2 expression beyond the level induced by PTBP1 downregulation.

208

209 **Functional significance of PTBP2 expression for neuronal conversion**

210 To probe the functional importance of PTBP2 expression, we performed the knockdown

211 experiments of PTBP2 with an shRNA during neuronal conversion. PTBP2 shRNA completely

212 impaired the induction of neurons marked by the loss of MAP2 expression, a neuronal marker

213 (Figure 3E). The effect of shRNA was specific to PTBP2 knockdown as supplementing *PTBP2*

214 cDNA rescued the reprogramming defect (Figure 3E). These findings were somewhat surprising

215 as the results from a previous study indicated that reduction of PTBP2 by shRNA was found to
216 promote maturation of reprogrammed neurons (Xue et al. 2016). It is not clear why shRNA-
217 versus miRNA-based reprogramming approaches lead to these conflicting results. Our results,
218 however, clearly demonstrate the essential role of PTBP2 at the onset of neuronal conversion.
219 Furthermore, knocking down PTBP2 in primary cultured human neurons resulted in increased
220 cell death as measured with SYTOX assay (Figure S4A-B), consistent with results from previous
221 studies that demonstrated the essential function of PTBP2 in primary neurons (Li et al., 2014).
222 To further gain insights into PTBP2 function during neuronal conversion, we performed
223 Human Clariom D Assay in HAFs expressing the non-specific control miR-NS, miR-9/9*-124,
224 or miR-9/9*-124 with PTBP2 shRNA to identify genes whose expression and alternative splicing
225 patterns were affected by the reduction of PTBP2. By two weeks, miR-9/9*-124-expressing cells
226 showed significant downregulation of *PTBP1* and other non-neuronal fibroblast genes (*FBN1*
227 and *S100A4*), and upregulation of *PTBP2* and neuronal genes (*NEFM,* and *SNAP25*) in
228 comparison to the control miR-NS expression (FC $\geq$ 1.5, ANOVA p-value < 0.05) (Figure S4C)
229 (Abernathy et al., 2017). To examine the alternative splicing events mediated by PTBP2 during
230 neuronal reprogramming, differentially spliced events were compared between PTBP2 shRNA
231 and control shRNA (shCTL) conditions in the miR-9/9*-124 expression background. We found
232 that reducing PTBP2 led changes in splicing events (-2 $\leq$ splicing index $\geq$ 2, ANOVA p-value <
233 0.05) indicated by red (positive splicing index) and green dots (negative splicing index) (Figure
234 S4D). This analysis identified some of the known splicing targets of PTBP2, such as the exon
235 skipping or exclusion in *UNC13B*, *DLG4*, and *CADM3*, and inclusion in *DNM1* and *SMARCC2*
236 transcripts (Figure S4D) (Li et al., 2014; Licatalosi et al., 2012; Vuong et al., 2016; Zheng et al.,
237 2012). Comparing genes upregulated in response to miR-9/9*-124 to genes associated with
238 PTBP2-mediated alternative splicing (differential splicing events between miR-9/9*-124 shCTL

239 and shPTBP2 conditions), identified 1183 differentially spliced transcripts of genes involved in
240 processes such as neuronal differentiation and signaling (Figure S4E) (Table S2). Altogether, our
241 results support the role of PTBP2 as a crucial regulator of the neuronal program during the
242 neuronal conversion of HAFs.
243
244 **Differential sequence composition between PTBP1 and PTBP2 3'UTRs**
245 We sought to identify effectors that promote miR-124 function in enhancing PTBP2 expression.
246 RNA-binding proteins (RBPs) have been shown to interact with miRNA-loaded RISC
247 complexes to modulate target gene expression (Iadevaia and Gerber, 2015; Jiang and Coller,
248 2012; Plass et al., 2017). We ran the sequence of *PTBP2* 3'UTR under three RBP motif
249 prediction databases, including RBPDB (Cook et al., 2011), RBPmap (Paz et al., 2014), and
250 beRBP (Yu et al., 2018) (Figure S5A). Across the three databases, two RBPs, ELAVL1 and
251 PUM2, were consistently predicted to bind to *PTBP2* 3'UTR (Figure S5A). As PTBP2 is
252 neuronal-enriched, we focused on the family of RBPs in which ELAVL1 belongs to, the
253 ELAVL-family proteins known to include neuron-specific homologs. Both the expression of
254 *ELAVL1* and Pumilio family RBPs, *PUM2* or its homolog, *PUM1*, are not specific to neurons
255 (Lin et al., 2018; Okano and Darnell, 1997; Spassov and Jurecic, 2002). *ELAVL1* is known to be
256 ubiquitously expressed while the other three family members, *ELAVL2*, *ELAVL3*, and *ELAVL4*
257 (collectively referred to as neuronal *ELAVLs*, *nELAVLs*), are neuron-specific (Okano and
258 Darnell, 1997). As *PTBP2* is a neuronal gene, we reasoned that nELAVLs would be concurrently
259 enriched and bind to *PTBP2* 3'UTR as ELAVLs share RNA-binding domains (Okano and
260 Darnell, 1997). We examined the HITS-CLIP data of nELAVLs in the human brain (Scheckel et
261 al., 2016) and found nELAVLs to be highly enriched at *PTBP2* 3'UTR, in contrast to *PTBP1*
262 3'UTR (Figure S5B-C). This selective binding is likely due to the presence of AU-rich elements

263 (AREs) within *PTBP2* 3'UTR since ELAVLs have been shown to bind to AREs (Ince-Dunn et
264 al., 2012; Scheckel et al., 2016), and *PTBP1* 3'UTR lacks the ARE (Figure S5B). Moreover, the
265 binding of nELAVLs mapped to the ARE directly upstream of the first miR-124 site (s1; seed,
266 highlighted in red) within the 3'UTR of *PTBP2* (Figure S5C).

267 To examine if nELAVLs are induced during neuronal conversion, we measured the
268 expression of ELAVL-family binding proteins as well as other brain-enriched RBPs, including
269 NOVA-, RBFOX-family proteins, and SSRM4 by qPCR. We found that miNs express the
270 neuronal RBPs similarly to the human brain, such as the selective upregulation of nELAVLs, in
271 contrast to the ubiquitous expression of *ELAVL1* (Figure 4A) (Okano and Darnell, 1997). To
272 determine if nELAVL induction occurs concurrently with PTBP2 upregulation, we assessed
273 ELAVL expression at multiple time points during the neuronal conversion. We found that the
274 transcriptional activation of nELAVLs, with *ELAVL3* being the most robust one (blue), aligned
275 with the upregulation of *PTBP2* (black) by nine days into reprogramming (Figure 4B).
276

277 **MiRNA-mediated PTBP2 induction requires ELAVL3 binding at PTBP2 3'UTR**

278 We then tested whether ARE within *PTBP2* 3'UTR would serve as a sequence that binds
279 ELAVL proteins by expressing 3'UTRs of *PTBP1*, *PTBP2,* or *PTBP2* without ARE
280 (PTBP2ΔARE 3'UTR) with individual FLAG-tagged ELAVLs (ELAVL1-4) in HEK293T cells
281 (Figure 4C). RNA-immunoprecipitation (RIP) of FLAG-ELAVLs with FLAG antibody,
282 followed by qPCR for detecting the loaded 3'UTRs using primers specific for either *PTBP1* or
283 *PTBP2* 3'UTRs displayed significant enrichment for *PTBP2* 3'UTR with nELAVL (ELAVL2, 3,
284 and 4) pull-downs, while the binding of ELAVL1 to *PTBP2* 3'UTR was minimal. We could not
285 detect significant enrichment for *PTBP1* 3'UTR for any of the ELAVLs (Figure 4C).
286 Importantly, deleting ARE in *PTBP2* 3'UTR (PTBP2ΔARE 3'UTR) abolished the binding of

287 nELAVL proteins to *PTBP2* 3'UTR (Figure 4C) indicating that the ARE within *PTBP2* 3'UTR
288 serves to recruit nELAVLs.
289 We asked whether adding nELAVLs to the non-neuronal context of HEK293T cells,
290 thereby reconstituting nELAVLs that become available during neuronal conversion, would
291 alleviate miR-124-mediated repression of PTBP2 and enhance PTBP2 expression instead.
292 Adding individual ELAVLs to control *PGK1* 3'UTR had no effect on luminescence (relative
293 luminescence of ~ 1; *PGK1* 3'UTR histograms) (Figure 4D). Luciferase activities with *PTBP1*
294 3'UTR remained repressed upon miR-9/9*-124 expression compared to the control miR-NS
295 irrespective of the ELAVL addition (relative luminescence of < 1; *PTBP1* 3'UTR histograms)
296 (Figure 4D). MiR-9/9*-124 led to the repression *PTBP2* 3'UTR in the absence of ELAVLs
297 (black, relative luminescence ratio < 1; *PTBP2* 3'UTR histograms) (Figure 4D). However,
298 adding ELAVL2 (green) and ELAVL3 (blue) significantly alleviated miR-9/9*-124-mediated
299 repression on *PTBP2* 3'UTR, with especially ELAVL3 (blue) having the most significant effect
300 on elevating the luciferase activity in comparison to the control construct (Figure 4D). To
301 examine the requirement of ARE, we repeated the ELAVL addition experiments using the
302 luciferase cassette with *PTBP2* 3'UTR lacking the ARE sequence (*PTBP2ΔARE*). Deleting ARE
303 abolished the effect of ELAVL3 (blue) on *PTBP2* (*PTBP2ΔARE* 3'UTR histograms), which
304 stayed repressed (Figure 4D), demonstrating the direct role of ELAVL3 at ARE of *PTBP2*
305 3'UTR in modifying the function miR-124.
306
307 **Selective activity of ELAVL3 on PTBP2 3'UTR is dependent on the hinge region**
308 ELAVL1-4 members exhibit high sequence homology across all three functional RNA
309 recognition motifs (RRMs) except for the non-conserved spacer region (also referred to as hinge
310 region) flanked by RRM2 and RRM3 (Hinman et al., 2013; Okano and Darnell, 1997). To better

311 understand the specificity of ELAVL3 on *PTBP2* 3'UTR regulation, we mutagenized the hinge
312 region of ELAVL1 and ELAVL3 by deleting or swapping the hinge region (H) between
313 ELAVL1 and ELAVL3. Deleting the H in *ELAVL3* (*ELAVL3ΔH*) (light blue) abrogated the
314 alleviating effect on *PTBP2* 3'UTR repression, whereas no effect was observed with *PGK1*
315 3'UTR (Figure 4E, *PGK1* 3'UTR histograms). Moreover, replacing the *ELAVL3* H with *ELAVL1*
316 H (*ELAVL3-E1H*) (dark blue) still led to the failure of alleviating the *PTBP2* 3'UTR repression
317 (Figure 4E), and none of the *ELAVL3* variants (wild-type and mutants) had any effect on
318 *PTBP2ΔARE* 3'UTR (Figure 4E, *PTBP2ΔARE* 3'UTR histograms). These results indicate that
319 the specificity of ELAVL3 to *PTBP2* 3'UTR is mediated by the *ELAVL3* H region. This notion
320 is further supported by the increase in the luminescence readout of *PTBP2* 3'UTR in HEK293T
321 cells when *ELAVL1* H is replaced by *ELAVL3* H (*ELAVL1-E3H*) (dark red) compared to wild-
322 type *ELAVL1* (red) (Figure 4F, *PTBP2* 3'UTR histograms). Our results altogether uncover the
323 specificity of ELAVL3 in promoting PTBP2 expression.
324
325 **Synergism between nELAVL and AGO requires miR-124 site in PTBP2 3'UTR**
326 We further tested whether the miR-124 sites within *PTBP2* 3'UTR would also be critical for
327 mediating the PTBP2 upregulation with ELAVL3. By mutating the miR-124 seed-match
328 sequences within *PTBP2* 3'UTR (*PTBP2Δs1s2* 3'UTR), adding ELAVLs failed to enhance the
329 luciferase activity over the control (CTL, black; relative luminescence ratio unchanged;
330 *PTBP2Δs1s2* 3'UTR histograms) (Figure 5A). This result is in contrast to wild-type *PTBP2*
331 3'UTR where ELAVL3 can enhance luciferase activity in the presence of miR-124 target sites
332 (Figures 4D, 5A). Interestingly, the lack of the increased luminescence with ELAVL3 addition
333 was not due to the failure of ELAVL binding to *PTBP2Δs1s2* 3'UTR because qPCR analysis

334 with nELAVL-RIP showed persistent binding of ELAVLs to *PTBP2Δs1s2* 3'UTR (Figure 5B).
335 These results altogether suggest the requirement of both ARE and miR-124 sites in *PTBP2*
336 3'UTR for PTBP2 upregulation (Figure 5C).
337
338 **ELAVL3 promotes PTBP2 expression during neuronal reprogramming**
339 To further examine if ELAVL3 would be critical for inducing PTBP2 expression during the
340 neuronal conversion of HAFs, we performed ELAVL3 knockdown by shRNA (shELAVL3) to
341 assess PTBP2 expression and neuronal reprogramming. Knocking down ELAVL3 resulted in the
342 significant downregulation of PTBP2 expression as determined by immunostaining, qPCR, and
343 immunoblotting analyses, and impairment of the conversion process (Figures 6A-C). This
344 knockdown effect was specific for ELAVL3 downregulation as PTBP2 expression and neuronal
345 fate acquisition could be rescued by overexpressing *ELAVL3* cDNA with shELAV3 (Figures 6A-
346 B). It is noteworthy that reducing the function of other nELAVLs (ELAVL2 and 4) had only a
347 minor effect on PTBP2 expression (Figures 6B-C), highlighting the role of ELAVL3 as a
348 primary driver for PTBP2 upregulation with miR-124.
349
350 **MiR-124 and nELAVL interaction for other neuronal transcripts**
351 To gain insights into whether the synergism of miR-124 and ELAVLs for miRNA-mediated
352 upregulation would be unique for PTBP2 or a broader mechanism to other neuronal genes, we
353 carried out a comparative analysis between multiple datasets: i) the previously identified DEGs
354 upregulated in response to miR-9/9*-124 at day 20 into reprogramming (Abernathy et al. 2017),
355 ii) DEGs bound by AGO HITS-CLIP (Figure 1), and iii) DEGs responsive to miR-124 tough
356 decoy (Figure 2), to iv) genes bound by nELAVLs in the human brain (Scheckel et al., 2016)
357 (Figure 6D). These multiple comparisons identified 54 genes, including *PTBP2* (Table S3),

358 enriched for neuronal biological terms generally involved in synaptic processes (Figure 6D).
359 Examples of these identified genes include *MAP2*, *SEMA6A, RCAN2, DOCK3*, *SCN1A*, and
360 *CAMK1D,* some of which some we showed as targets of miR-124 (Figure 2, Table S3). Although
361 the additional identified targets remain to be further dissected for the functional meaning
362 underlying the upregulation, our findings pointing to these transcripts harboring both AGO-miR-
363 124 and nELAVL binding sites suggest that the synergistic activities of miR-124 and nELAVL
364 for promoting gene expression may extend to other genes important for neuronal differentiation
365 and function (Figure 6E).
366

367 **Discussion**

368 In the present study, we uncovered the role of miR-124 in the upregulation of genes associated
369 with neuronal differentiation and function during the neuronal conversion of human fibroblasts.
370 This finding provides insights into the function of miRNAs in addition to their canonical role as
371 a repressor of downstream target genes. Of the bound AGO transcripts are *bona fida* miR-124
372 target genes in which the 3'UTRs can be repressed in a non-neuronal context, but reverses upon
373 neuronal induction. By examining the mutually exclusive regulation of *PTBP1* and *PTBP2*, we
374 reveal how miR-124 plays a bifunctional role depending on the sequence composition at the
375 3'UTR, the availability of neuronal ELAVLs, and the interaction with AGOs to mediate the
376 switching of PTB homolog expression during the neuronal conversion of HAFs. Although we
377 focus specifically on the interplay between miR-124 and ELAVL3 for PTBP2 upregulation,
378 future studies should also examine if other RBPs can also synergize with AGOs for such target
379 gene regulation. For example, FXR1, an RBP, has been shown in previous studies to interact
380 with AGOs to facilitate gene expression in non-neuronal cells (Truesdell et al., 2012; Vasudevan
381 et al., 2007; Vasudevan and Steitz, 2007).

382 The selective role of ELAVL3, and not ubiquitous ELAVL1 or neuronal-specific
383 ELAVL2 and ELAVL4, in mediating PTBP2 induction in neurons highlights the functional
384 specificity of ELAVL family members in neurons. Like ELAVL3, ELAVL1 binds AREs and has
385 been shown to interact with RISC components (Kim et al., 2009; Vasudevan and Steitz, 2007).
386 Our results, however, clearly defines the functional specificity inherent in ELAVL3 that cannot
387 be replaced by ELAVL1, especially for regulating PTBP2 expression with miR-124. We found
388 that the specificity is, at least in part, driven by the hinge region inferred by the region-swapping
389 experiments between ELAVL1 and ELAVL3. As there is no known ARE recognition unique to
390 each ELAVL family member, it is likely that interactors associating with the hinge region may
391 be regulating ELAVL specificity and targeting (Fujiwara et al., 2012; Hinman et al., 2013).
392 To investigate if the synergism of miR-124 and nELAVLs for transcript stabilization and
393 activation can be generalized to other neuronal transcripts beyond *PTBP2*, we examined the
394 existing nELAVL HITS-CLIP dataset and uncovered that miR-124- and nELAVL-mediated
395 upregulation of target transcripts may not be a unique occurrence to *PTBP2*, but likely an
396 overlooked mechanism that maintains gene expression in neurons. Interestingly, as we identified
397 numerous neuronal genes to be targets of miR-124, in addition to *PTBP2*, such as *MAP2,*
398 *RCAN2, and SEMA6A*, we argue that miR-124 may be critical for enhancing the overall neuronal
399 program. This notion also indicates that miR-9/9*-124 is highly neurogenic as these miRNAs not
400 only allow for the conversion of HAFs into neurons (Abernathy et al. 2017; Yoo et al. 2011), but
401 also enhanced the expression of neuronal markers, such as *MAP2*, when overexpressed during
402 neuronal differentiation of human pluripotent stem cell-derived neurons (Ishikawa et al., 2020;
403 Sun et al., 2016). Although further tests are required to see if all the identified transcripts
404 targeted by both miR-124 and nELAVLs share the same mechanism as PTBP2, our results from
405 miR124-TuD and its effect on other neuronal genes lend support to the general role of miR-124

406 as a positive regulator of some its target genes in neurons. Future experiments taking a closer
407 look at RNA structure, motif proximity with RBPs, and additional interacting proteins will
408 provide further mechanistic insights to how a single miRNA can simultaneously repress and
409 activate different transcripts in a cell context-dependent manner.

410 Our study offers insights into the bifunctional mode of miR-124 conferring miRNAs as a
411 reprogramming effector that can contribute to the neuronal program by upregulating specific
412 neuronal genes. As miRNAs have been typically checked for their targets in non-neuronal cell
413 lines, it is plausible that the dual-mode of miRNAs may not be unique to miR-124 in neurons,
414 but instead utilized and altered in other cellular contexts with the help of other cell type-specific
415 RBPs. The governance of miRNA activity by the sequences within 3'UTR highlights the role of
416 cell type-specific RBPs as core regulators of gene expression.

417

418 **Materials and Methods**

419 **Cell culture**

420 Primary human fibroblasts used in this study was from a 22-year-old female (GM02171, NIGMS
421 Coriell Institute for Medical Research) while human neonatal fibroblasts (ScienCell, 2310) was
422 used exclusively for the HITS-CLIP experiment. Primary human neurons were obtained
423 commercially (ScienCell, 1520) with gender and age of the source undisclosed. Fibroblasts were
424 maintained in high glucose Dulbecco's Modified Eagle Medium (Gibco, 11960044) containing
425 10% FBS (Gibco, 10437028), MEM non-essential amino acids (Gibco, 11140050), sodium
426 pyruvate (Gibco, 11360070), GlutaMAX (Gibco, 35050061), HEPES (Gibco, 15630080),
427 penicillin-streptomycin (Gibco, 15130122), and 2-mercaptoethanol (Gibco, 21985023) at 37°C.
428 Human neurons were maintained in neuronal media (NM; ScienCell, 1521) at 37°C.

429 Lenti-X 293T (Clontech, 632180) cells were maintained in high glucose Dulbecco's
430 Modified Eagle Medium (Gibco, 11960044) containing 10% FBS (Gibco, 10437028), MEM
431 non-essential amino acids (Gibco, 11140050), sodium pyruvate (Gibco, 11360070), GlutaMAX
432 (Gibco, 35050061), HEPES (Gibco, 15630080), penicillin-streptomycin (Gibco, 15130122), and
433 2-mercaptoethanol (Gibco, 21985023) at 37°C.
434 Primary mouse cortical neurons were maintained in Neurobasal-A medium (Gibco,
435 10888022), B-27 plus supplement (Gibco, A3582801), GlutaMAX (Gibco, 35050061), and
436 penicillin-streptomycin (Gibco, 15130122) at 37°C.
437
438 **MiR-9/9*-124-mediated neuronal conversion**
439 To initiate reprogramming, doxycycline-inducible pT-BclXL-miR-9/9*-124 (Addgene, 60857)
440 and reverse tetracycline-controlled transactivator rtTA (Addgene, 66810) lentivirus with 8
441 ug/mL polybrene (Sigma, H9268) was added to a plate of confluent fibroblasts and spinfected at
442 37°C for 30 min at 1,000xG. Full media change with 1 μg/mL doxycycline (DOX; Sigma-
443 Aldrich, D9891) occurred the following day. Two days following transduction, cells underwent
444 another media change supplemented with DOX and respective antibiotics (Puromycin, Life
445 Technologies, A11138-03; Blasticidin S HCl, Life Technologies, A11139-03). Five days after
446 transduction, cells were plated onto poly-l-ornithine (Sigma-Aldrich, P4957), fibronectin
447 (Sigma-Aldrich, F4759), and laminin (Sigma-Aldrich, L2020) coated coverslips or onto 10cm^2
448 Primaria plates (Corning, 353803) followed by full media switch to neuronal media (NM;
449 ScienCell, 1521) the next day supplemented with 200 μM dibutyl-cyclic AMP (cAMP; Sigma-
450 Aldrich, D0627), 1 mM valproic acid (VPA; Sigma Aldrich, P4543), 10 ng/mL human BDNF
451 (PeproTech, 450-02), 10 ng/mL human NT-3 (Peprotech, 450-03), 1 μM retinoic acid (RA;

452 Sigma-Aldrich, R2625), RevitaCell supplement (Gibco, A2644501), and antibiotics. DOX was
453 supplemented every 2 days while half media changes occurred every 4 days until day 30.
454
455 **Plasmids and cloning**
456 For luciferase assay, full length 3'UTR of target transcripts were cloned and ligated into
457 pmirGLO vector. For mutagenizing miR-124 target sites, QuikChange XL site-directed
458 mutagenesis kit (Agilent, 200516) was used according to the manufacturer's protocol. Using the
459 same UTR sequences, 3'UTR was attached immediately downstream of a destablized EGFP
460 reporter and subcloned into lentiviral vector. Sequences for shRNAs were synthesized through
461 Integrated DNA Technologies, annealed, and ligated into the pLKO.1 vector (Addgene, 8453 or
462 26655). Overexpression vectors of either lentiviral (N106 or N174) or mammalian expression
463 (pcDNA3.1+, Invtrogen, V79020) was cut using NotI cut site (NEB, R0189) for insert ligation.
464 Tough decoy for miR-124 was synthesized (GeneScript) and subcloned into pLemir vector using
465 MluI (NEB, R0198) and NotI sites.
466
467 **Lentivirus production**
468 Lentivirus was produced as previously described (Richner et al., 2015). Briefly, 1.5 μg pMD2.G,
469 4.5 μg psPAX2, 6 μg of plasmid in lentiviral backbone, 600 μl Opti-MEM (Life Technologies,
470 31985) and 48 μl of 2 mg/mL polyethyleneimine (PEI; Polysciences, 24765) were mixed and
471 transfected into Lenti-X 293T (Clontech, 632180) plated at $6x10^6$ cells per 10 cm^2 dish. Media
472 was changed the following day, and viral supernatant was collected, filtered and spun at
473 70,000xG for 2 hr at 4°C two days later. The viral pellet collected per 10 cm^2 dish was
474 resuspended in 1 mL PBS.

475

476 **Immunostaining analysis**

477 Cells were fixed with 4% paraformaldehyde (PFA; Electron Microscopy Sciences, 15710) for 20
478 mins at room temperature (RT) followed by three washes with PBS. Cells were permeabilized
479 and blocked in 0.3% TritonX-100, 2% normal goat serum (NGS; Jackson ImmunoResearch
480 Laboratories, 005-000-121) and 5% bovine serum albumin (BSA; Sigma-Aldrich, A7906) in
481 PBS for 1 hr at RT prior to incubation with primary antibodies overnight at 4°C. After three
482 washes with PBS, cells were incubated with respective secondary antibodies for 1 hr at RT.
483 Coverslips were mounted onto coverslides with ProLong Gold antifade reagent (Invitrogen,
484 P36934) for imaging using Leica SP5X white light laser confocal system with Leica Application
485 Suite (LAS) Advanced Fluorescence. See Supplemental Table S4 for a list of antibodies used.

486

487 **SYTOX assay**

488 SYTOX assay was performed as previously described (Victor et al., 2018). Briefly, 0.1 μM
489 SYTOX gene nucleic acid stain (Invitrogen, S7020) and 1 μl/mL of Hoeschst 33342 (Thermo
490 Scientific, 66249) were added into cell medium. Samples were incubated for at least 15 mins in
491 37°C prior to imaging. Images were taken using Leica DMI 4000B inverted microscope with
492 Leica Application Suite (LAS) Advanced Fluorescence.

493

494 **Luciferase assay**

495 HEK 293 cells plated in 96-well plate were transfected with 100 ng of pSilencer-miRNA, 100 ng
496 of pmirGLO containing 3'UTR of interest, and PEI (Polysciences, 24765) with Opti-MEM (Life
497 Technologies, 31985). Forty-eight hours after transfection, luciferase activity was assayed using

498 Dual-Glo luciferase assay system (Promega, E2920) according to the manufacturer's protocol
499 using Synergy H1 Hybrid plate reader (BioTek). Luciferase activity was obtained by normalizing
500 firefly luminescence to renilla luminescence (luciferase activity = firefly/renilla) followed by
501 normalizing to respective pSilencer-miR-NS control.
502
503 **Flow cytometry**
504 Destabilized EGFP reporter with or without 3'UTR of interest was transduced into HEK 293
505 cells to establish a stable reporter containing cell line with Blasticidin S HCl (Life Technologies,
506 A11139-03) selection. The day following transduction with miR-9/9*-124 lentivirus, media was
507 changed with the addition of DOX (Sigma-Aldrich, D9891). At day 3, media change was
508 supplemented with DOX and puromycin (Life Technologies, A11138-03). DOX was
509 supplemented every 2 days following transduction. At day 10, cells were imaged, and collected
510 for flow cytometry. Briefly, cells were collected in PBS and incubated with propidium iodide
511 (PI; Sigma-Aldrich, P4861) on ice until ready. Using FACSCalibur (BD Biosciences), all PI-
512 negative cell population was obtained for the gating of GFP-negative and -positive cell
513 population.
514
515 **Quantitative reverse transcription PCR**
516 Total RNA of cells was extracted using TRIzol Reagent (Invitrogen, 15596026). Reverse
517 transcription was performed using SuperScript III first strand synthesis system for RT-PCR
518 (Invitrogen, 18080-051) according to the manufacturer's protocol from fibroblasts,
519 reprogrammed neurons, and human brain total RNA (Invitrogen, AM7962). Quantitative PCR
520 was performed using SYBR Green PCR master mix (Applied Biosystems, 4309155) and

521 StepOnePlus Real-Time PCR system (Applied Biosystems, 4376600) according to the
522 manufacturer's protocol against target genes.
523
524 **HITS-CLIP**
525 AGO HITS-CLIP was performed on cells after 2 weeks into reprogramming of miR-NS or miR-
526 9/9*-124-expressing neonatal fibroblasts (ScienCell, 2310). Cells were harvested, UV-
527 crosslinked, lysed, and processed according to Moore et al. 2014. Briefly, cross-linked cells were
528 lysed and treated with RQ1 DNase (Promega, M6101) and RNaseA (Thermo). Complex
529 containing AGO-miRNA-mRNA were immunoprecipitated overnight at 4°C with pan-AGO
530 antibody. The immunoprecipitated complex was radio-labelled and extracted after running on
531 NuPAGE gel (Thermo). RNA from the 130kDa band was extracted for sequencing using TruSeq
532 Small RNA Library Preparation Kits (San Diego, CA). Samples were sequences using Illumina
533 HiSeq 2500 platform at the Genome Technology Access Center (GTAC) at Washington
534 University School of Medicine, St. Louis.
535
536 **MiRNA Tough Decoy**
537 Total RNA was extracted from day 20 cells expressing miR-9/9*-124 + TuD-miR-NS, and miR-
538 9/9*-124 + TuD-miR-124 using TRIzol Reagent (Invitrogen, 15596026) in combination with
539 RNeasy micro kit (Qiagen, 74004). RNA quality (RIN > 9.6) was determined with 2100
540 Bioanalyzer (Agilent) and samples underwent low input Takara-Clontech SMARTer kit (Takara,
541 639490) library preparation. Samples were sequenced using NovaSeq S4 and processed at the
542 Genome Technology Access Center (GTAC) at Washington University School of Medicine, St.
543 Louis.
544

545 **Human Clariom D Microarray**

546 For Human Clariom D Array (Affymetrix), total RNA was extracted from day 14 cells
547 expressing miR-NS, miR-9/9*-124 + shCTL, and miR-9/9*-124 + shPTBP2 using TRIzol
548 Reagent in combination with RNeasy mini kit (Qiagen, 74104). RNA quality (RIN > 9.6) was
549 determined with 2100 Bioanalyzer and samples (biological duplicates each) underwent
550 amplification and hybridization according to manufacturer's protocol by GTAC at Washington
551 University School of Medicine, St. Louis.

552

553 **Immunoblot analysis**

554 Cells were lysed with sonication (Diagenode, UCD-200) in RIPA buffer (Thermo Scientific,
555 89900) supplemented with protease inhibitor cocktail tablet (Roche, 04693132001). Protein
556 concentration of cleared lysate was measured using Pierce BCA protein assay kit (Thermo
557 Scientific, 23227) and read with Synergy H1 Hybrid plate reader (BioTek). Lysate and sample
558 buffer (Life Technologies, NP0008) were boiled, separated with Bis-Tris gels, and transferred to
559 nitrocellulose membrane (GE Healthcare Life Sciences, 10600006). Membrane was blocked with
560 5% milk for 1 hr at RT and incubated with primary antibody overnight at 4°C. After three
561 washes of TBST (1X TBS and 0.1% Tween-20), the membrane was incubated with respective
562 horseradish peroxidase-conjugated antibody for 1 hr at RT followed by three washes with TBST.
563 Blots were developed with ECL system (Thermo Scientific, 34580) and imaged or developed
564 onto film. See Supplemental Table S3 for a list of antibodies used.

565

566 **Immunoprecipitation analysis**

567 Cells were lysed with sonication (Diagenode, UCD-200) in IP buffer (20 mM HEPES, 150 mM
568 NaCl, 10% glycerol, 5 mM EDTA, 1% Triton X-100) supplemented with protease inhibitor

569 cocktail tablet (Roche, 04693132001). Cleared lysate was incubated with anti-FLAG M2
570 magnetic beads (Sigma-Aldrich, M8823) overnight with rotation at 4°C. The beads were washed
571 three times with IP buffer and bound proteins were boiled and eluted with sample buffer (Life
572 Technologies, NP0008), separated with Bis-Tris gels, and immunoblotted.
573
574 **RNA-IP**
575 Following immunoprecipitation with anti-FLAG magnetic beads (Sigma-Aldrich, M8823) or
576 anti-V5 antibody (Invitrogen, MA5-15253) coupled to Dynabeads protein G (Life Technologies,
577 NP10003D), beads were resuspended in 90 ul of IP buffer with proteinase K (NEB, P8107S) for
578 30 mins at 37°C. To extract RNA, 1 mL of TRIzol Reagent (Invitrogen, 15596026) was added to
579 the bead slurry. Final RNA was DNase I (Invitrogen, 18068015) treated prior to RT-qPCR.
580
581 **GO enrichment analysis**
582 Gene ontology analyses were performed using Metascape (Tripathi et al., 2015) with minimum
583 overlap of 3, P value cutoff of 0.01, and minimum enrichment of 1.5. Entire gene list was used
584 for each GO analysis.
585
586 **RNAhybrid miRNA-target duplex analysis**
587 To predict the presence of miR-124-3p binding sites at HITS-CLIP peaks, peak sequences were
588 extracted by on the genomic coordinates and processed through RNAhybrid (Rehmsmeier, 2004)
589 against miR-124-3p miRNA sequence with at least a free energy threshold of -20 kcal/mol.
590
591 **RBP binding analysis**

592 RNA-binding protein prediction database/software, RBPDB (Cook et al., 2011)), RBPmap (Paz
593 et al., 2014), and beRBP (Yu et al., 2018) for *PTBP2* 3'UTR sequence were used. Default
594 criteria were selected for all three software for non-bias prediction of any human RBP motifs.
595
596 **Data Analyses**
597 AGO HITS-CLIP reads for miR-NS and miR-9/9*-124-expressing cells at least two
598 weeks into reprogramming were trimmed and aligned to human genome hg38 using STAR with
599 default parameters. Aligned reads at CDS and UTRs were binned at a continuously 100 bp bins.
600 Two separate sets of bins were generated of which the two sets are offset by 50 bp in order to
601 capture all alignments. Aligned reads were quantified using featureCounts and differentially
602 present bins or peaks were determined using DESeq2 with the following criteria: adj. p-value <
603 0.05 and LogFC of ≤ -2 and ≥ 2. HITS-CLIP datasets will be publicly available.
604 RNA-seq for day 20 miNs expressing either CTL TuD-miR-NS or TuD-miR-124 was
605 analyzed by GTAC's RNA-seq pipeline. Briefly, reads were aligned to hg38 with STAR and
606 processed through EdgeR to obtain differentially expressed genes with adj. p-value of < 0.05.
607 RNA-seq dataset consisting of TuD-miR-NS and TuD-miR-124 at day 20 will be publicly
608 available.
609 Human Clariom D Array data was analyzed using manufacturer's software, Expression
610 Console followed by Transcriptome Analysis Console (TAC). For gene level analysis, genes
611 comparing miR-9/9*-124 vs miR-NS linear fold change of ≥ 1.5 and ANOVA P < 0.05 were
612 considered to upregulated in neuronal conditions. For splicing analysis, splicing events with
613 linear splicing index ≤ -2 and ≥ 2, ANOVA P < 0.05 were considered significant splicing events.
614 Human Clariom D array dataset consisting of miR-NS, miR-9/9*-124 with shCTL, and miR-
615 9/9*-124 with shPTBP2 at day 14 will be publicly available.

616

617 **Author Contributions**

618 Y.L.L. conducted experiments shown in Figures 2-5 and associated supplementary Figures 1, 3-
619 6. Y.J.L. conducted experiments shown in Figure 1 and supplementary Figure 2. A.S.Y.
620 supervised the study. Y.L.L. and A.S.Y. wrote the manuscript.

621

622 **Acknowledgements**

623 We thank the GTAC at Washington University for the sequencing service and support, and flow
624 Cytometry Core at Washington University for equipment use. We thank We thank P. Gontarz,
625 for the bioinformatics analysis of AGO HITS-CLIP, D. Annamalai and A. H. Kim for the help
626 with tough decoy designs, and K. Cates and L. Capano for the helpful suggestions with the
627 manuscript. Y.L.L. is supported by the LIFENAD Fellowship. This study was supported through
628 awards and funds to A.S.Y by the Andrew B. and Virginia C. Craig Faculty Fellowship
629 endowment, NIH Director's Innovator Award (DP2NS083372), Presidential Early Career Award
630 for Scientists and Engineers (PECASE), and NIH (RF1AG056296 and R01NS107488).

631

632 **Declaration of Interests**

633 The authors declare no competing interest.

634

635 **References**

636 Abernathy DG, Kim WK, McCoy MJ, Lake AM, Ouwenga R, Lee SW, Xing X, Li D, Lee HJ,
637 Heuckeroth RO, Dougherty JD, Wang T, Yoo AS. 2017a. MicroRNAs Induce a
638 Permissive Chromatin Environment that Enables Neuronal Subtype-Specific
639 Reprogramming of Adult Human Fibroblasts. *Cell Stem Cell* **21**:332-348.e9.
640 doi:10.1016/j.stem.2017.08.002

641 Bak RO, Hollensen AK, Primo MN, Sorensen CD, Mikkelsen JG. 2013. Potent microRNA
642 suppression by RNA Pol II-transcribed "Tough Decoy" inhibitors. *RNA* **19**:280–293.
643 doi:10.1261/rna.034850.112
644 Ballas N, Grunseich C, Lu DD, Speh JC, Mandel G. 2005. REST and Its Corepressors Mediate
645 Plasticity of Neuronal Gene Chromatin throughout Neurogenesis. *Cell* **121**:645–657.
646 doi:10.1016/j.cell.2005.03.013
647 Boutz PL, Stoilov P, Li Q, Lin C-H, Chawla G, Ostrow K, Shiue L, Ares M, Black DL. 2007. A
648 post-transcriptional regulatory switch in polypyrimidine tract-binding proteins
649 reprograms alternative splicing in developing neurons. *Genes & Development* **21**:1636–
650 1652. doi:10.1101/gad.1558107
651 Chen Y, Sun J, Chen W, Wu G, Wang Y, Zhu K, Wang J. 2019. miR-124/VAMP3 is a novel
652 therapeutic target for mitigation of surgical trauma-induced microglial activation. *Sig*
653 *Transduct Target Ther* **4**:27. doi:10.1038/s41392-019-0061-x
654 Cook KB, Kazan H, Zuberi K, Morris Q, Hughes TR. 2011. RBPDB: a database of RNA-
655 binding specificities. *Nucleic Acids Research* **39**:D301–D308. doi:10.1093/nar/gkq1069
656 Farrell BC, Power EM, Dermott KWM. 2011. Developmentally regulated expression of Sox9
657 and microRNAs 124,128 and 23 in neuroepithelial stem cells in the developing spinal
658 cord. *International Journal of Developmental Neuroscience* **29**:31–36.
659 doi:10.1016/j.ijdevneu.2010.10.001
660 Fujiwara T, Fukao A, Sasano Y, Matsuzaki H, Kikkawa U, Imataka H, Inoue K, Endo S,
661 Sonenberg N, Thoma C, Sakamoto H. 2012. Functional and direct interaction between
662 the RNA binding protein HuD and active Akt1. *Nucleic Acids Research* **40**:1944–1953.
663 doi:10.1093/nar/gkr979
664 Haraguchi T, Ozaki Y, Iba H. 2009. Vectors expressing efficient RNA decoys achieve the long-
665 term suppression of specific microRNA activity in mammalian cells. *Nucleic Acids*
666 *Research* **37**:e43–e43. doi:10.1093/nar/gkp040
667 Hinman MN, Zhou H-L, Sharma A, Lou H. 2013. All three RNA recognition motifs and the
668 hinge region of HuC play distinct roles in the regulation of alternative splicing. *Nucleic*
669 *Acids Research* **41**:5049–5061. doi:10.1093/nar/gkt166
670 Iadevaia V, Gerber A. 2015. Combinatorial Control of mRNA Fates by RNA-Binding Proteins
671 and Non-Coding RNAs. *Biomolecules* **5**:2207–2222. doi:10.3390/biom5042207
672 Ince-Dunn G, Okano HJ, Jensen KB, Park W-Y, Zhong R, Ule J, Mele A, Fak JJ, Yang C, Zhang
673 C, Yoo J, Herre M, Okano H, Noebels JL, Darnell RB. 2012. Neuronal Elav-like (Hu)
674 Proteins Regulate RNA Splicing and Abundance to Control Glutamate Levels and
675 Neuronal Excitability. *Neuron* **75**:1067–1080. doi:10.1016/j.neuron.2012.07.009
676 Ishikawa M, Aoyama T, Shibata S, Sone T, Miyoshi H, Watanabe H, Nakamura M, Morota S,
677 Uchino H, Yoo AS, Okano H. 2020. miRNA-Based Rapid Differentiation of Purified
678 Neurons from hPSCs Advancestowards Quick Screening for Neuronal Disease
679 Phenotypes In Vitro. *Cells* **9**:532. doi:10.3390/cells9030532
680 Jiang P, Coller H. 2012. Functional Interactions Between microRNAs and RNA Binding
681 Proteins. *MicroRNA e* **1**:70–79. doi:10.2174/2211536611201010070
682 Kim HH, Kuwano Y, Srikantan S, Lee EK, Martindale JL, Gorospe M. 2009. HuR recruits let-
683 7/RISC to repress c-Myc expression. *Genes & Development* **23**:1743–1748.
684 doi:10.1101/gad.1812509
685 Lee SW, Oh YM, Lu Y-L, Kim WK, Yoo AS. 2018. MicroRNAs Overcome Cell Fate Barrier by
686 Reducing EZH2-Controlled REST Stability during Neuronal Conversion of Human Adult
687 Fibroblasts. *Developmental Cell* **46**:73-84.e7. doi:10.1016/j.devcel.2018.06.007

688 Lessard J, Wu JI, Ranish JA, Wan M, Winslow MM, Staahl BT, Wu H, Aebersold R, Graef IA,
689 Crabtree GR. 2007. An Essential Switch in Subunit Composition of a Chromatin
690 Remodeling Complex during Neural Development. *Neuron* **55**:201–215.
691 doi:10.1016/j.neuron.2007.06.019
692 Li Q, Zheng S, Han A, Lin C-H, Stoilov P, Fu X-D, Black DL. 2014. The splicing regulator
693 PTBP2 controls a program of embryonic splicing required for neuronal maturation. *eLife*
694 **3**. doi:10.7554/eLife.01201
695 Licatalosi DD, Yano M, Fak JJ, Mele A, Grabinski SE, Zhang C, Darnell RB. 2012. Ptbp2
696 represses adult-specific splicing to regulate the generation of neuronal precursors in the
697 embryonic brain. *Genes & Development* **26**:1626–1642. doi:10.1101/gad.191338.112
698 Lin K, Zhang S, Shi Q, Zhu M, Gao L, Xia W, Geng B, Zheng Z, Xu EY. 2018. Essential
699 requirement of mammalian *Pumilio* family in embryonic development. *MBoC* **29**:2922–
700 2932. doi:10.1091/mbc.E18-06-0369
701 Makeyev EV, Zhang J, Carrasco MA, Maniatis T. 2007. The MicroRNA miR-124 Promotes
702 Neuronal Differentiation by Triggering Brain-Specific Alternative Pre-mRNA Splicing.
703 *Molecular Cell* **27**:435–448. doi:10.1016/j.molcel.2007.07.015
704 Moore MJ, Zhang C, Gantman EC, Mele A, Darnell JC, Darnell RB. 2014. Mapping Argonaute
705 and conventional RNA-binding protein interactions with RNA at single-nucleotide
706 resolution using HITS-CLIP and CIMS analysis. *Nat Protoc* **9**:263–293.
707 doi:10.1038/nprot.2014.012
708 Mucaj V, Lee SS, Skuli N, Giannoukos DN, Qiu B, Eisinger-Mathason TSK, Nakazawa MS,
709 Shay JES, Gopal PP, Venneti S, Lal P, Minn AJ, Simon MC, Mathew LK. 2015.
710 MicroRNA-124 expression counteracts pro-survival stress responses in glioblastoma.
711 *Oncogene* **34**:2204–2214. doi:10.1038/onc.2014.168
712 Okano HJ, Darnell RB. 1997. A Hierarchy of Hu RNA Binding Proteins in Developing and
713 Adult Neurons. *The Journal of Neuroscience* **17**:3024–3037.
714 doi:10.1523/JNEUROSCI.17-09-03024.1997
715 Packer AN, Xing Y, Harper SQ, Jones L, Davidson BL. 2008. The Bifunctional microRNA miR-
716 9/miR-9* Regulates REST and CoREST and Is Downregulated in Huntington's Disease.
717 *Journal of Neuroscience* **28**:14341–14346. doi:10.1523/JNEUROSCI.2390-08.2008
718 Paz I, Kosti I, Ares M, Cline M, Mandel-Gutfreund Y. 2014. RBPmap: a web server for mapping
719 binding sites of RNA-binding proteins. *Nucleic Acids Research* **42**:W361–W367.
720 doi:10.1093/nar/gku406
721 Plass M, Rasmussen SH, Krogh A. 2017. Highly accessible AU-rich regions in 3' untranslated
722 regions are hotspots for binding of regulatory factors. *PLOS Computational Biology*
723 **13**:e1005460. doi:10.1371/journal.pcbi.1005460
724 Rehmsmeier M. 2004. Fast and effective prediction of microRNA/target duplexes. *RNA*
725 **10**:1507–1517. doi:10.1261/rna.5248604
726 Richner M, Victor MB, Liu Y, Abernathy D, Yoo AS. 2015. MicroRNA-based conversion of
727 human fibroblasts into striatal medium spiny neurons. *Nature Protocols* **10**:1543–1555.
728 doi:10.1038/nprot.2015.102
729 Scheckel C, Drapeau E, Frias MA, Park CY, Fak J, Zucker-Scharff I, Kou Y, Haroutunian V,
730 Ma'ayan A, Buxbaum JD, Darnell RB. 2016. Regulatory consequences of neuronal
731 ELAV-like protein binding to coding and non-coding RNAs in human brain. *eLife* **5**.
732 doi:10.7554/eLife.10421

733 Schoenherr C, Anderson D. 1995. The neuron-restrictive silencer factor (NRSF): a coordinate
734 repressor of multiple neuron-specific genes. *Science* **267**:1360–1363.
735 doi:10.1126/science.7871435
736 Spassov DS, Jurecic R. 2002. Cloning and comparative sequence analysis of PUM1 and PUM2
737 genes, human members of the Pumilio family of RNA-binding proteinsq 10.
738 Staahl BT, Tang J, Wu W, Sun A, Gitler AD, Yoo AS, Crabtree GR. 2013. Kinetic Analysis of
739 npBAF to nBAF Switching Reveals Exchange of SS18 with CREST and Integration with
740 Neural Developmental Pathways. *Journal of Neuroscience* **33**:10348–10361.
741 doi:10.1523/JNEUROSCI.1258-13.2013
742 Sun AX, Yuan Q, Tan S, Xiao Y, Wang D, Khoo ATT, Sani L, Tran H-D, Kim P, Chiew YS,
743 Lee KJ, Yen Y-C, Ng HH, Lim B, Je HS. 2016. Direct Induction and Functional
744 Maturation of Forebrain GABAergic Neurons from Human Pluripotent Stem Cells. *Cell*
745 *Reports* **16**:1942–1953. doi:10.1016/j.celrep.2016.07.035
746 Sun Y, Luo Z-M, Guo X-M, Su D-F, Liu X. 2015. An updated role of microRNA-124 in central
747 nervous system disorders: a review. *Front Cell Neurosci* **9**. doi:10.3389/fncel.2015.00193
748 Tripathi S, Pohl MO, Zhou Y, Rodriguez-Frandsen A, Wang G, Stein DA, Moulton HM,
749 DeJesus P, Che J, Mulder LCF, Yángüez E, Andenmatten D, Pache L, Manicassamy B,
750 Albrecht RA, Gonzalez MG, Nguyen Q, Brass A, Elledge S, White M, Shapira S,
751 Hacohen N, Karlas A, Meyer TF, Shales M, Gatorano A, Johnson JR, Jang G, Johnson T,
752 Verschueren E, Sanders D, Krogan N, Shaw M, König R, Stertz S, García-Sastre A,
753 Chanda SK. 2015. Meta- and Orthogonal Integration of Influenza "OMICs" Data Defines
754 a Role for UBR4 in Virus Budding. *Cell Host & Microbe* **18**:723–735.
755 doi:10.1016/j.chom.2015.11.002
756 Truesdell SS, Mortensen RD, Seo M, Schroeder JC, Lee JH, LeTonqueze O, Vasudevan S. 2012.
757 MicroRNA-mediated mRNA Translation Activation in Quiescent Cells and Oocytes
758 Involves Recruitment of a Nuclear microRNP. *Scientific Reports* **2**.
759 doi:10.1038/srep00842
760 Tsutsui Ken, Tsutsui Kimiko, Sano K, Kikuchi A, Tokunaga A. 2001. Involvement of DNA
761 Topoisomerase IIβ in Neuronal Differentiation. *Journal of Biological Chemistry*
762 **276**:5769–5778. doi:10.1074/jbc.M008517200
763 Vasudevan S, Steitz JA. 2007. AU-Rich-Element-Mediated Upregulation of Translation by
764 FXR1 and Argonaute 2. *Cell* **128**:1105–1118. doi:10.1016/j.cell.2007.01.038
765 Vasudevan S, Tong Y, Steitz JA. 2007. Switching from Repression to Activation: MicroRNAs
766 Can Up-Regulate Translation. *Science* **318**:1931–1934. doi:10.1126/science.1149460
767 Victor MB, Richner M, Olsen HE, Lee SW, Monteys AM, Ma C, Huh CJ, Zhang B, Davidson
768 BL, Yang XW, Yoo AS. 2018. Striatal neurons directly converted from Huntington's
769 disease patient fibroblasts recapitulate age-associated disease phenotypes. *Nature*
770 *Neuroscience*. doi:10.1038/s41593-018-0075-7
771 Visvanathan J, Lee S, Lee B, Lee JW, Lee S-K. 2007. The microRNA miR-124 antagonizes the
772 anti-neural REST/SCP1 pathway during embryonic CNS development. *Genes &*
773 *Development* **21**:744–749. doi:10.1101/gad.1519107
774 Vuong JK, Lin C-H, Zhang M, Chen L, Black DL, Zheng S. 2016. PTBP1 and PTBP2 Serve
775 Both Specific and Redundant Functions in Neuronal Pre-mRNA Splicing. *Cell Reports*
776 **17**:2766–2775. doi:10.1016/j.celrep.2016.11.034
777 Watanabe M, Tsutsui Ken, Tsutsui Kimiko, Inoue Y. 1994. Differential expressions of the
778 topoisomerase IIa and IIb mRNAs in developing rat brain. *Neuroscience Research*
779 **19**:51–57.

780 Xue Y, Qian H, Hu J, Zhou B, Zhou Y, Hu X, Karakhanyan A, Pang Z, Fu X-D. 2016.
781 Sequential regulatory loops as key gatekeepers for neuronal reprogramming in human
782 cells. *Nature Neuroscience* **19**:807–815. doi:10.1038/nn.4297
783 Yoo AS, Staahl BT, Chen L, Crabtree GR. 2009. MicroRNA-mediated switching of chromatin-
784 remodelling complexes in neural development. *Nature* **460**:642–646.
785 doi:10.1038/nature08139
786 Yoo AS, Sun AX, Li L, Shcheglovitov A, Portmann T, Li Y, Lee-Messer C, Dolmetsch RE,
787 Tsien RW, Crabtree GR. 2011. MicroRNA-mediated conversion of human fibroblasts to
788 neurons. *Nature* **476**:228–231. doi:10.1038/nature10323
789 Yu H, Wang J, Sheng Q, Liu Q, Shyr Y. 2018. beRBP: binding estimation for human RNA-
790 binding proteins. *Nucleic Acids Research*. doi:10.1093/nar/gky1294
791 Zheng S, Gray EE, Chawla G, Porse BT, O'Dell TJ, Black DL. 2012. PSD-95 is post-
792 transcriptionally repressed during early neural development by PTBP1 and PTBP2.
793 *Nature Neuroscience* **15**:381–388. doi:10.1038/nn.3026
794

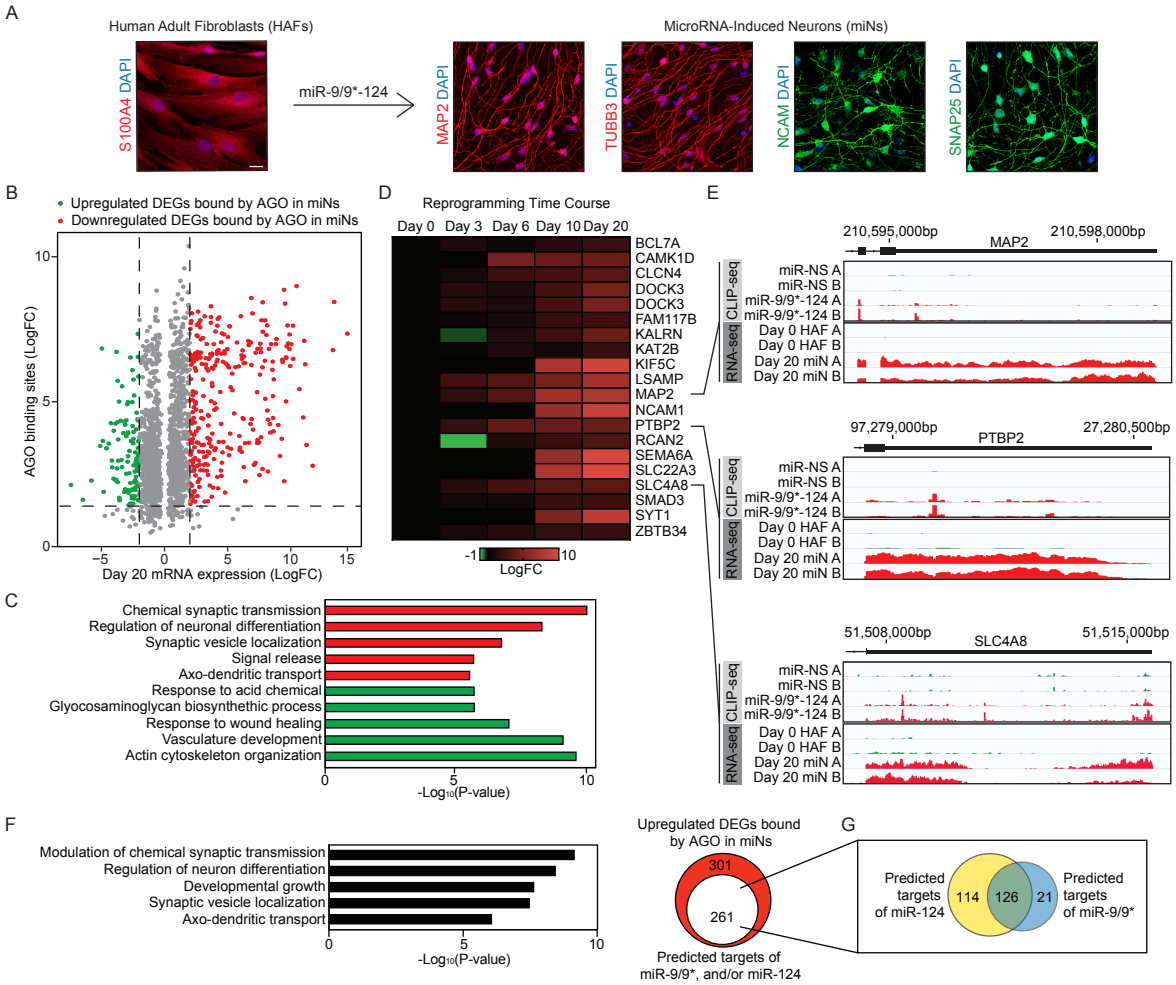

Figure 1. Enrichment of AGO binding on transcripts of neuronal genes upregulated during miR-9/9*-124-mediated neuronal conversion

(A) Examples of miR-9/9*-124-mediated direct reprogramming of human adult dermal fibroblasts (HAFs) into neurons (miNs). Photographs show immunostaining of the fibroblast marker (S100A4) and neuronal markers (MAP2, TUBB3, NCAM, and SNAP25). Scale bar = 20 µm.

(B) A volcano plot of differentially expressed genes at day 20 miNs and enrichment of AGO binding in response to miR-9/9*-124 expression identified by AGO HITS-CLIP analysis. Red dots, day 20 mRNA expression Log2FC ≥ 2; adj.P-value < 0.05, AGO binding Log2FC ≥ 2, adj.P-value < 0.05. Green dots, day 20 mRNA expression Log2FC ≤ 2; adj.P-value < 0.05, AGO binding Log2FC ≥ 2, adj.P-value < 0.05.

(C) Top biological GO terms of upregulated (red) and downregulated (green) DEGs in day 20 miNs differentially bound by AGO.

(D) Time course heatmap of select upregulated DEGs enriched for AGO binding with miR-9/9*-124 expression.

(E) Track views of AGO CLIP-seq tracks (top) and RNA-seq tracks (bottom) for gene examples showing the enrichment of AGO binding miR-9/9*-124 expression (over control miR-NS) and increased transcript levels at 3'UTRs.

(F) Of the 301 unique upregulated DEGs identified in (A), 261 are predicted to harbor miR-9/9* and/or miR-124 sites at the AGO-enriched regions through RNAhybrid prediction. The graph indicates top biological GO terms associated with the 261 upregulated DEGs containing miR-9/9* and/or miR-124 target sites.

(G) Breakdown of the 261 upregulated DEGs in (F) based on common or specific targets of miR-9/9* and/or miR-124.

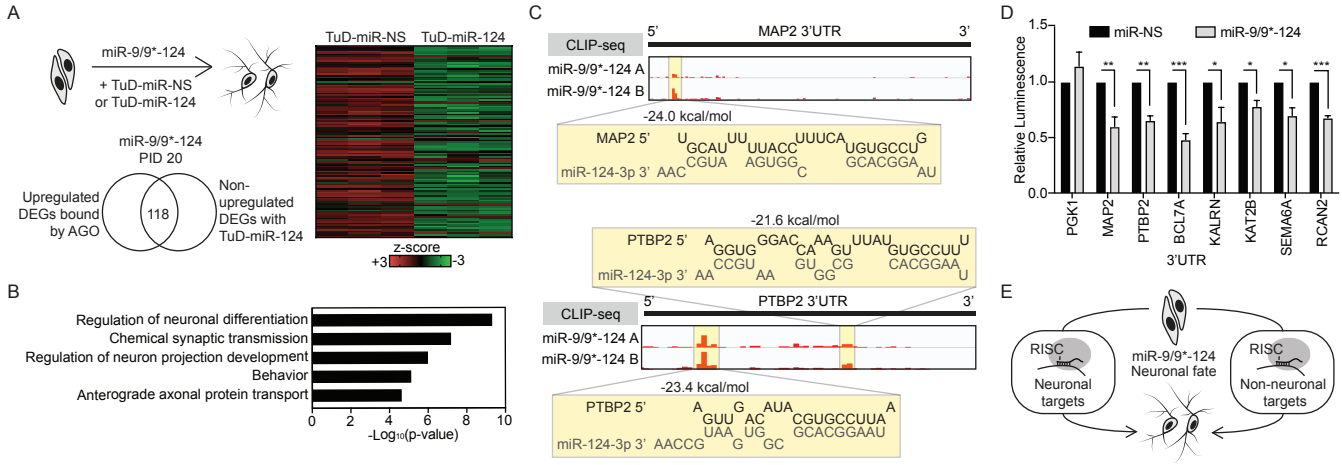

Figure 2. Identification of miR-124 target genes that fail to be upregulated upon the inhibition of miR-124 during miRNA-mediated neuronal conversion

(A) Left, miR-124 activity is reduced through the use of tough decoy (TuD). By overlapping with upregulated DEGs bound by AGO (Figure 1), 118 genes were identified as genes that fail to be increased upon the reduction of miR-124. Right, a heatmap of z-scores of the 118 genes from RNA-seq comparing miNs between TuD-miR-NS and TuD-miR-124 treatments.

(B) Top biological GO terms associated with the 118 genes identified in (A).

(C) Predicted binding of miR-124 to the 3'UTR sequences of neuronal target genes, for example, *MAP2* and *PTBP2*, according to RNAhybrid prediction at the highlighted AGO HITS-CLIP peaks.

(D) Luciferase assays in HEK293T cells of upregulated neuronal target genes of miR-124 selected from A). In the non-neuronal context of HEK293T cells, 3'UTRs from the neuronal genes are targeted and repressed, instead, by miR-9/9*-124. Luminescence measured after 48 hrs of transfection and normalized to miR-NS control of each condition. Data are represented by mean ± SEM from three independent experiments (from left, ** P = 0.0094, P = 0.0011; *** P < 0.001; * P = 0.048, 0.015, 0.012; *** P < 0.001).

(E) A diagram of the observed phenomenon in which miR-9/9*-124 can promote neuronal identity by simultaneously targeting both non-neuronal genes for repression while promoting the expression of neuronal genes during neuronal conversion.

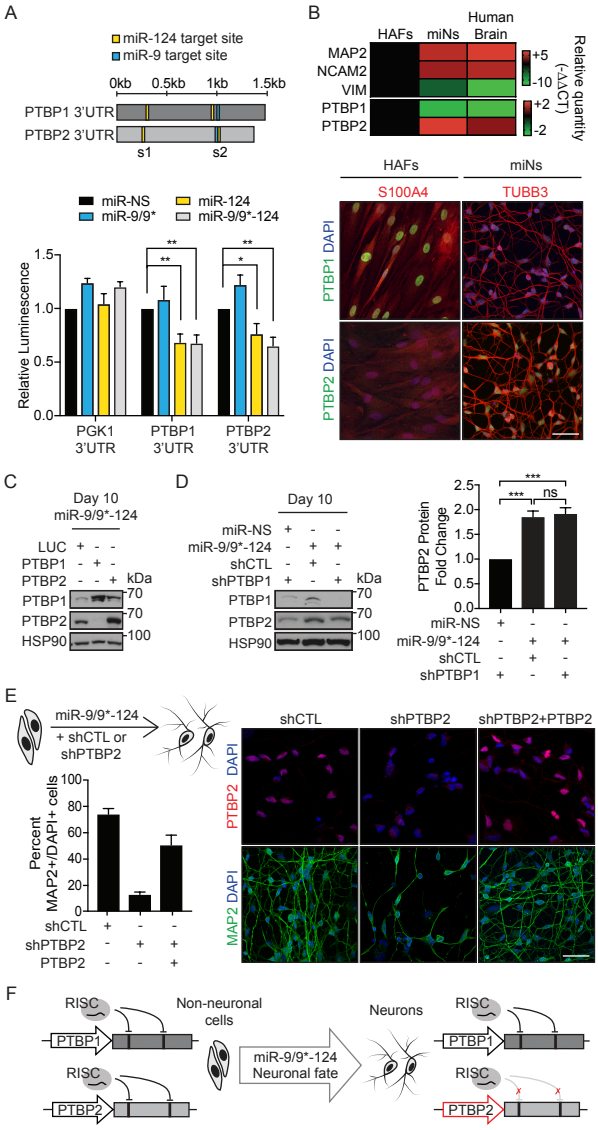

Figure 3. MiR-124 targets both PTBs, but differentially regulate PTB expression during neuronal conversion.
(A) Top, a schematic diagram of PTB 3'UTRs with miR-124 (yellow) and miR-9 (blue) target sites. S1 and s2 refer to the two conserved miR-124 target sites on PTBP2 3'UTR. Bottom, luciferase assays with luminescence measured after 48 hrs of transfection and normalized to miR-NS control in each condition. Data are represented by mean ± SEM from four independent experiments. Two-way ANOVA followed by Dunnett's test (from left, PTBP1 3'UTR ** P = 0.0043, 0.0034; PTBP2 3'UTR * P = 0.0355, ** P = 0.0016)
(B) Top, A heatmap of gene expression assessed by qPCR in starting HAFs, day 30 miRNA-induced neurons (miNs), and human brain RNA. Bottom, PTB switching is recapitulated during the miRNA-mediated direct conversion of HAFs into neurons. HAFs and day 30 miNs immunostained for PTBP1 and PTBP2, along with a fibroblast marker, S100A4, and a pan-neuronal marker, TUBB3. Scale bar = 50 μm.
(C) Initial induction of PTBP2 by the reduction of PTBP1 by either shRNA or miRNAs during miRNA-mediated neuronal reprogramming. PTBP1 overexpression in the miR-9/9*-124 expression background suppresses the PTBP2 induction.
(D) Left, an immunoblot showing that PTBP1 knockdown in HAFs resulted in induction of PTBP2, but PTBP2 expression becomes more pronounced in the presence of miR-9/9*-124 compared to PTBP1 knowdown only. Right, quantification of PTBP2 band intensity as relative fold changes compared to PTBP1 knockdown alone. Data were normalized to HSP90 from four independent experiments. The plots were represented in mean ± SEM. One-way ANOVA followed by Tukey's test (from top *** P = 0.0002, 0.0004; ns P = 0.8925).
(E) Top left, a schematic diagram of the experimental procedure. Right, photographs of day 30 miNs treated with CTL shRNA, PTBP2 shRNA, or PTBP2 shRNA with PTBP2 cDNA. Cells were immunostained for PTBP2 and MAP2. Bottom left, quantification of the percentage of MAP2-positive cells with two or more neurite processes over the total number of DAPI-positive cells. Scale bar = 50 μm. Data are represented as mean ± SEM. One-way ANOVA followed by Tukey's test (*** P < 0.0001; ** P 0.0016). shCTL n = MAP2 356/482; shPTBP2 n = MAP2 31/239; shPTBP2+PTBP2 n = MAP2 225/454.
(F) A model of differential miR-124 activity on PTB 3'UTRs during neuronal conversion.

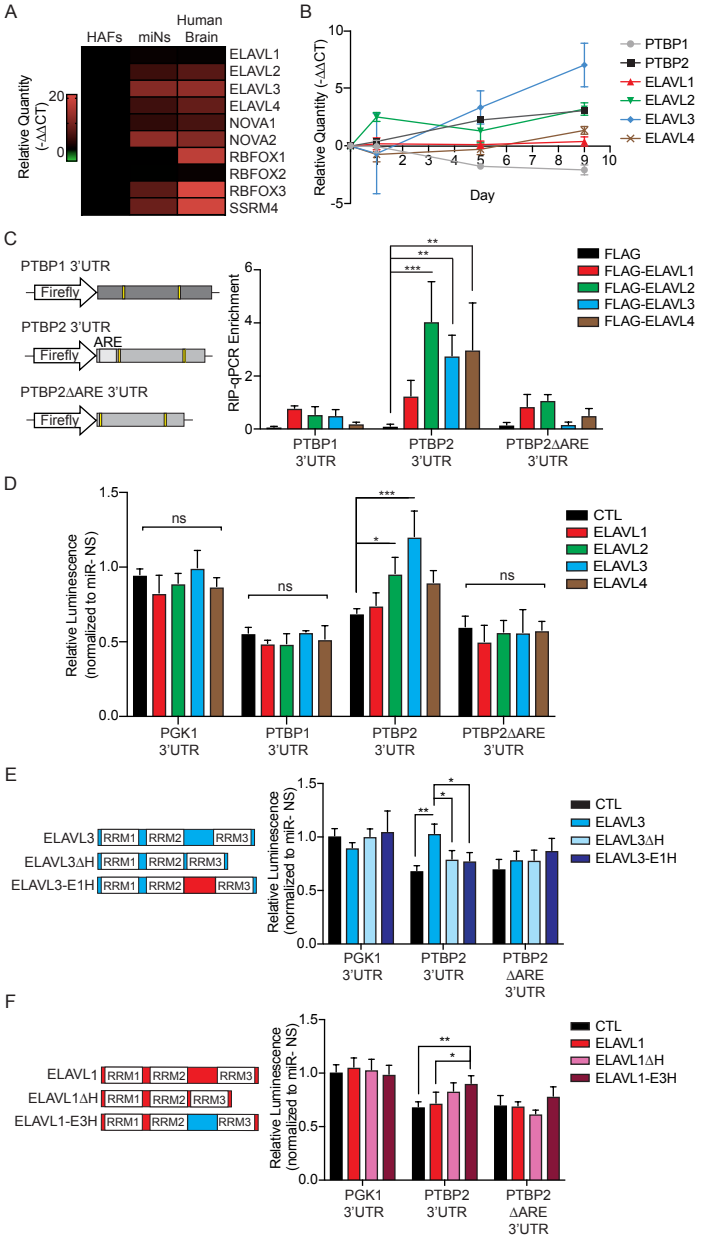

Figure 4. MiRNA-mediated PTBP2 upregulation requires nELAVL binding at PTBP2 3'UTR

(A) An expression heatmap of neuronal-enriched RBPs determined by qPCR in starting HAFs, day 20 miNs, and human brain RNA.

(B) Time course qPCR assays of PTB and ELAVL transcripts during neuronal reprogramming.

(C) Left, a diagram of luciferase constructs containing different PTB 3'UTRs: PTBP1 3'UTR, and PTBP2 3'UTR with and without (PTBP2ΔARE) the AU-rich element (ARE) used for RIP and luciferase assays. Right, RIP of individual FLAG-tagged ELAVLs 48 hrs after transfection. Enrichment normalized to input determined by qPCR for PTBP1 or PTBP2 3'UTR. Data are represented by mean ± SEM from three independent experiments. Two-way ANOVA followed by Dunnett's test (from left, PTBP2 3'UTR *** P = 0.0001, ** P = 0.0086, 0.0042).

(D) Luciferase assays with the addition of individual ELAVLs in the luciferase constructs containing the control PGK1, PTBP1, PTBP2 or PTBP2ΔARE 3'UTR. Luminescence was measured 48 hrs after the transfection and normalized miR-9/9*-124 to miR-NS control of each condition. Data are represented by mean ± SEM from at least three independent experiments. Two-way ANOVA followed by Dunnett's test (* P = 0.0312, *** P = 0.0001).

(E) Left, a schematic diagrm of ELAVL3 hinge mutants. Right, luciferase assays with the addition of wild-type ELAVL3 or ELAVL3 hinge mutants (ELAVL3Δ H: ELAVL3 hinge deletion; ELAVL3-E1H: ELAVL3 with ELAVL1 hinge). Luminescence was measured 48 hrs after transfection and normalized miR-9/9*-124 to miR-NS control of each condition. Data are represented by mean ± SEM from at least four independent experiments. Two-way ANOVA followed by Tukey's test (from left ** P = 0.0020, * P = 0.0435, * P = 0.0286).

(F) Left, a schematic diagram of ELAVL1 hinge mutants. Right, luciferase assays with the addition of wild-type ELAVL1 or ELAVL1 hinge mutants (ELAVL1 ΔH: ELAVL1 hinge deletion; ELAVL1-E3H: ELAVL1 with ELAVL3 hinge). Luminescence was measured 48 hrs after transfection and normalized miR-9/9*-124 to miR-NS control of each condition. Data represented in mean ± SEM from at least four independent experiments. Two-way ANOVA followed by Tukey's test (** P = 0.0069, * P = 0.0260).

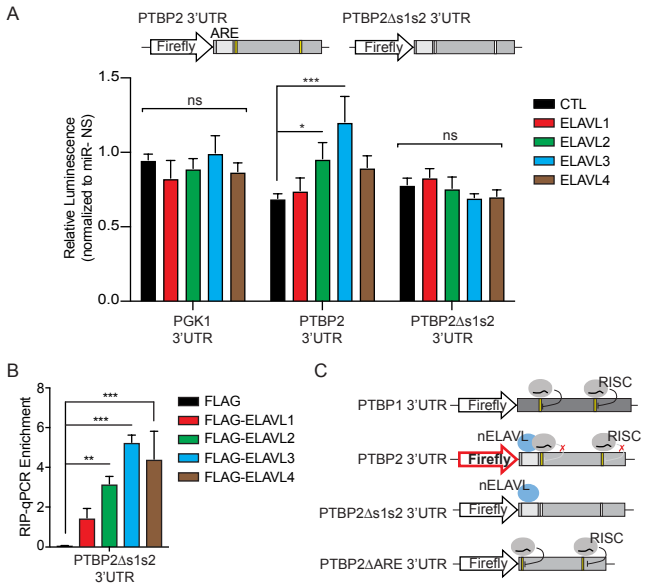

Figure 5. Synergism of nELAVL and miR-124 on PTBP2 3'UTR
(A) Top, a diagram of luciferase constructs containing PTBP2 3'UTR with or without miR-124 sites (PTBP2Δ s1s2). Bottom, luciferase assays with the addition of individual ELAVLs in PGK1 control, PTBP2, or PTBP2Δ s1s2 3'UTR. Luminescence was measured 48 hrs after transfection and normalized miR-9/9*-124 to miR-NS control of each condition. Data are represented by mean ± SEM from at least three independent experiments.Two-way ANOVA followed by Dunnett's test (* P = 0.0312, *** P = 0.0001).
(B) RIP of individual FLAG-tagged ELAVLs in PTBP2Δs1s2 3'UTR 48 hrs after transfection. Enrichment normalized to input determined through qPCR against PTBP2 3'UTR. Data are represented by mean ± SEM from three independent experiments. Two-way ANOVA followed by Dunnett's test (from left, PTBP2Δs1s2 3'UTR ** P = 0.0018, *** P = 0.0001, *** P = 0.0001).
(C) A schematic summary of nELAVL and RISC activities on PTB 3'UTRs.

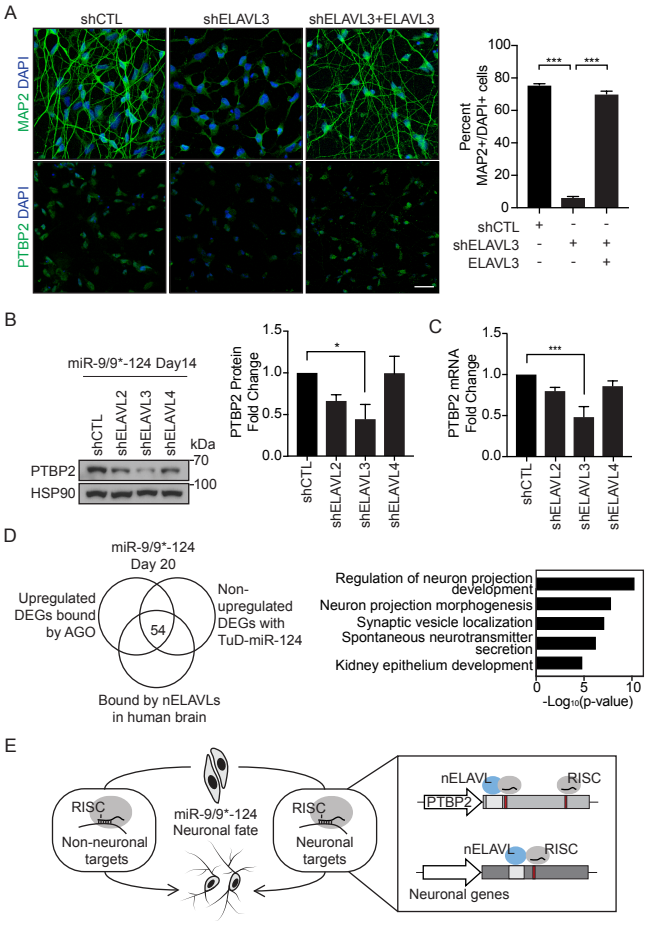

Figure 6. PTBP2 upregulation during reprogramming requires ELAVL3

(A) Left, day 30 miNs with shRNA knockdown against CTL, ELAVL3, and ELAVL3 with ELAVL3 cDNA rescue. Cells were immunostained for MAP2 and PTBP2. Scale bar 50 = µm. Right, quantification of the percentage of MAP2-positive cells over the total number of DAPI-positive cells with two or more neurites (left). Data represented as mean ± SEM. One-way ANOVA followed by Tukey's test (from left, *** P < 0.0001, *** P < 0.0001). shCTL n = MAP2 803/1060; shELAVL3 n = MAP2 67/1052; shELAVL3 + ELAVL3 n = MAP2 431/617.

(B) Left, immunoblot analysis of PTBP2 in day14 miNs with knockdown against CTL, ELAVL2, ELAVL3, and ELAVL4. Right, quantification of the PTBP2 band intensity as a relative fold change compared to shCTL normalized to HSP90 in four independent experiments. Data are represented by mean ± SEM. One-way ANOVA followed by Dunnett's test (* P = 0.0422).

(C) The relative quantity of PTBP2 transcript upon individual nELAVL knockdown compared to CTL at day14 miNs determined by qPCR. Data are represented by mean ± SEM from 3 independent experiments. One-way ANOVA followed by Dunnett's test (*** P = 0.0001).

(D) Left, a Venn diagram of day 20 upregulated DEGs bound by AGO identified by AGO HITS-CLIP in miNs overlapped with nELAVL-bound targets in the human brain. Right, top biological GO terms associated with the 54 genes that are predicted to be upregulated in miNs and targeted by both AGO and nELAVLs (left).

(E) A model of miR-9/9*-124 activity in simultaneously repressing non-neuronal targets while promoting the expression of select neuronal targets, such as PTBP2, for the successful acquisition of neuronal identity during the neuronal conversion of HAFs.